ISSN 0022-4766, Journal of Structural Chemistry, 2020, Vol. 61, No. 7, pp. 1145-1154. © Pleiades Publishing, Ltd., 2020.
Text © The Author(s), 2020, published in Zhurnal Strukturnoi Khimii, 2020, Vol. 61, No. 7, pp. 1208-1217.

CRYSTAL STRUCTURE AND ANTICANCER ACTIVITY ON RETINOBLASTOMA OF AN In(III)–Na(I) COORDINATION POLYMER BASED ON FLEXIBLE 4,4′-DITHIODIBENZOIC ACID

H. Guo[1], W.-Z. Zhan[1], S. Tang[1], Y. Wang[1], Y. Peng[1], L. Wang[1], W.-H. Chen[2], and L. Ye[1]*

A bimetallic coordination polymer is prepared via a hydrothermal reaction of H_2ddBA and $In(NO_3)_3$ in water with NaOH as a pH regulator. Its chemical formula is $[In_2Na(H_2O)_6(ddba)_3](NO_3)(H_2O)_7$ (**1**, H_2ddba = 4,4′-dithiodibenzoic acid). The composition and atomic arrangement of the prepared complexes are studied by the elemental analysis (EA) and the thermogravimetric analysis (TGA), powder and single crystal X-ray diffraction measurements. Moreover, a process of nanochemistry with oleic acid treatment at 453 K is used to produce nanostructure **1**. In the biological function detection, a miRNA relative expression is detected via RT-PCR and Bcl-2 expression level is determined with the Western blot. The Annexin V-FITC/PI staining is performed to detect retinoblastoma cell apoptosis after treatment with nano-**1**.

DOI: 10.1134/S0022476620070197

Keywords: coordination polymer, bimetallic, nanostructure, anticancer activity.

INTRODUCTION

Cancer poses a great threat to human health, killing millions of people every year [1]. Chemotherapy based on chemical anticancer drugs is still the main treatment [2]. Coordination chemistry has a great latent capacity to provide varieties of compounds that have multiple mechanisms associated with DNA binding, *redox* reactivity, and different geometries, some of which are specific to metals [3, 4]. In the past decades, the clinical success of cisplatin along with its analogues has aroused extensive interest in the research of novel metal-based anticancer drugs, however, its drug resistance, general toxicity, and serious side effects have severely limited its application [5]. As the research on coordination complexes with the antitumor activity has been deepening, different metal (except platinum) compounds are entering into clinical researches. Pharmaceutical and bioinorganic chemists are committed to designing as well as synthesizing novel metal-based anticancer agents which have a lower toxicity, better selectivity and biological activity along with different mechanisms to overcome the clinical problems of cisplatin analogues [6].

[1]Shenzhen Key Laboratory of Ophthalmology, Ocular Trauma Treatment and Stem Cell Differentiation Public Service Platform of Shenzhen, Shenzhen Eye Hospital, Affiliated Shenzhen Eye Hospital of Jinan University, Shenzhen, P. R. China; *lin_ye11@126.com. [2]Department of Oncology, The People′s Hospital of Changzhou, Changzhou, P. R. China.
Original article submitted September 28, 2019; revised November 14, 2019; accepted December 6, 2019.

Coordination polymers (CPs) are fully extended crystalline solids composed of multitopic organic connecters and metal ions. Over the past decades, they have attracted great research interest due to their latent applications and functional properties in many scientific fields. From these characteristics, many potential applications can be inferred, including chemical catalysis, molecular separation, gas storage, biomedicine as well as sensing [79]. CPs generally reveal an extremely low solubility in ordinary organic solvents, which restricts their usability in many ideal biological applications, including cancer diagnosis, drug delivery, imaging, and so on. One possible solution is to decrease the CP size to the nanoscale in order to easily manage nanoscale CPs (NCPs) in cells [10]. NCP is a hybrid material that combines the advantages of organic as well as inorganic nanoparticles. Compared with existing nanosystems, NCP has many advantages since its composition, shape, and size can be easily adjusted with the directional structure, highly porous and synthesis operation to obtain effective load characteristics. In addition, NCP is biodegradable in nature because the metal-ligand bond is unstable in nature, therefore, after its biological function, it can be easily discharged from the system [11]. On the other hand, mercaptan has abundant redox chemistry, which can induce a disulfide bond formation or reduce cracking according to different reaction media. In different acidic or alkaline media, at room temperature or under solvothermal conditions, many CPs have been generated using bisdentate disulfide ligands. In addition, the high glutathione (GSH) concentration in cancer cells could also lead to the disconnection of the S–S bond [12]. A bimetallic CP was triumphantly prepared via the hydrothermal reaction of H_2DDBA and $In(NO_3)_3$ in water with NaOH as a pH regulator. Its chemical formula was $[In_2Na(H_2O)_6(ddba)_3](NO_3)(H_2O)_7$ (**1**, H_2ddba = 4,4′-dithiodibenzoic acid). The composition and atomic arrangement of the prepared complexes were studied with the elemental analysis (EA) and the thermogravimetric analysis (TGA), powder and single crystal X-ray diffraction measurements. Moreover, a process of sonochemistry with oleic acid therapy at 298 K was used to produce nano-**1**. In the biological function detection, the RT-PCR results of the miRNA expression indicated that nano-**1** reduced the miRNA expression in a dose-dependent manner. The Western blot data revealed that the Bcl-2 expression level was increased by treating with nano-**1**. The Annexin V-FITC/PI staining results indicated that nano-**1** had excellent induction of apoptosis in retinoblastoma cells.

EXPERIMENTAL

Chemicals and measurements. All chemicals are available to be purchased at the market and can be utilized without further purification. A PerkinElmer model 240C instrument was used to document EA (N, H, and C). The morphologies of these two nanostructures were photographed by a JEOL JEM-2010F electron microscope. Utilizing a Rigaku 3III/D/Max diffractometer, the X-ray powder diffraction pattern was measured. TGA was carried out under a nitrogen atmosphere utilizing a NETZSCH STA 449C microanalyzer at a 10 °C/min heating rate.

Preparation of CP 1 and nano-1. We mixed NaOH (0.008 g, 0.2 mmol), H_2ddba (0.0304 g, 0.1 mmol) with $In(NO_3)_3{\cdot}6H_2O$ (0.0306 g, 0.1 mmol) at the 1:1:1 molar ratio to form a mixture, and stirred it. Water (10 mL) was added in half an hour in air; then the mixture was heated in a 25-mL Teflon-lined pure steel container to 140 °C for 96 h and sealed. After cooling to room temperature with a 5 K/h rate, yellow block crystals were gained in *ca*. 64% yield which was on the ground of In. Anal. $C_{42}H_{50}In_2NNaO_{28}S_6$ (1461) (%): C 34.51, H 3.45, N 2.96. Found (%): C 34.35, H 3.71, N 3.23.

Utilizing the sonochemical method to prepare NCP **1** nanorods, a high-density ultrasonic probe was immersed directly into the solution of $In(NO_3)_3{\cdot}6H_2O$ (0.0306 g, 0.1 mmol) and H_2ddba (0.1 mmol, 0.0306 g) in double-distilled water, and then an appropriate amount of a water solution (0.01 M, 5 mL) containing NaOH was added to this solution. Using a 12 W power ultrasound, the solution was irradiated for 1 h. The precipitates were screened and then washed by double-distilled water and dried in the air.

Crystal structure and refinement. Single crystal X-ray diffraction analysis of compound **1** was carried out using an Agilent Xcalibur Eos Gemini diffractometer with a Mo X-ray source (MoK_α, $\lambda = 0.71073$ Å). The successive Fourier difference synthesis and direct methods were applied to figure out the structures along with the full matrix least square approach on F^2 for their refinement with anisotropic thermal parameters of all non-hydrogen atoms based on the SHELX

software [13]. Because of a high disorder of water molecules in the lattice along with a low occupancy of NO_3^- ions, we could not exactly assign their atoms from the electronic maps via the structural refinement, therefore their electronic contributions were removed by the squeeze manipulation embedded in the PLATON software. The final chemical formula of **1** was determined by combining EA and single crystal X-ray diffraction, charge balance considerations as well as energy-dispersive X-ray spectrometry. The refinement results and crystallographic parameters are summarized in Table 1.

CCK-8 detection. To evaluate the nano-**1** inhibitory function on 5-Fu resistance in retinoblastoma cells, the CCK-8 method was carried out under manufacture′s instruction. In brief, the difference cancer cells at a logarithmic growth stage were collected and inoculated into 6-well plates with the final density of $5 \cdot 10^5$ cells per well. Then nano-**1**, buffer, ligand, and $In(NO_3)_3 \cdot 6H_2O$ solutions as well as the positive anticancer drug 5-Fu were added for 24 h treatment. Subsequently, the absorbance of each well was measured, and the results were presented as mean±SD.

Annexin V-FITC/PI apoptosis analysis. After treating with nano-**1**, the Annexin V-FITC/PI staining (BD Biosciences, New Jersey, USA) was conducted to evaluate the percentage of apoptotic SO-RB50, HXO-RB44, and y79 retinoblastoma cells under the guidance of the instructions with a minor modification. In brief, SO-RB50, HXO-RB44, and y79 retinoblastoma cells in the logarithmic growth phase were collected and seeded into 6-well plates at the final density of $1 \cdot 10^6$ cells/well. All the cells were cultured in an incubator at 37 °C, 5% CO_2 overnight. When the cells stepped into the logarithmic stage with the confluence reaching 70-80%, they were treated with nano-**1** for 24 h. Then the cells were trypsinized, washed with pre-cooled PBS, and re-suspended in a 500 μL of the Annexin V binding buffer. Subsequently, SO-RB50, HXO-RB44, and y79 retinoblastoma cells were incubated with 5 μL of Annexin V-FITC and 5 μL of a propidium iodide (PI) solution for 15 min at 37 °C in dark place. The percentage of apoptotic cells was analyzed by flow cytometry (BD Via, New Jersey, USA) at an excitation wavelength of 488 nm and emission wavelengths of 525 nm and 625 nm. The results were analyzed using flow cytometry (FACSCalibur, BD Biosciences, USA). This experiment was performed in triplicate.

RT-PCR assay of the miR-16-1 expression. The miR-16-1 relative expression in cancer cells after treatment with nano **1** was detected by the reverse transcription-polymerase chain reaction according to manufacture′s instructions [14]. In brief, SO-RB50, HXO-RB44, and y79 retinoblastoma cells were implanted into 6-well plates with the concentration of $1 \cdot 10^5$ cells/well, then the cells were treated with nano-**1** of severe dilutions for one day. After treatment, the cells were

TABLE 1. Refinement Indices and Structural Parameters for Complex **1**

Parameter	**1**
Empirical formula	$C_{42}H_{50}In_2NNaO_{28}S_6$
Formula weight	1273.67
Temperature, K	293(2)
Crystal system	Cubic
Space group	*Pn*-3*n*
a, Å	22.0015(7)
V, Å^3	10650.2(10)
Z	8
ρ_{calc}, g/cm^3	1.589
μ, mm^{-1}	1.176
Data / restraints / parameters	1833 / 54 / 106
GOOF on F^2	1.024
Final *R* indexes ($I \geq 2\sigma(I)$]	$R_1 = 0.0631$, $wR_2 = 0.1669$
Final *R* indexes (all data)	$R_1 = 0.1006$, $wR_2 = 0.1968$
Largest diff. peak / hole, e/Å^3	0.81 / –0.51
CCDC	1952290

collected and total RNA was extracted via the TRIzol reagent under manufacturer′s instruction. The RNA concentration of different groups was measured by the OD260/OD280 ratio, and the RNA solution was sub-packaged and stored at –80 °C for the subsequent use. cDNA was synthesized via a High-Capacity cDNA Reverse Transcription Kit, and the SYBR Green Master Mix was carried out to detect the miR-16-1 relative expression using GAPDH as the internal control. The $2^{-\Delta\Delta Ct}$ method was used for the relative quantification in triplicate.

Western blot assay. As a mitochondrial outer membrane protein that blocks apoptosis death, the Bcl-2 protein expression level was further measured with the Western blot assay after treating with nano-**1** [15]. In short, SO-RB50, HXO-RB44, and y79 retinoblastoma cells were treated with nano-**1** for 24 h, and then harvested and lysed with lysis buffer. The protein concentration was measured with the BCA kit. The protein samples were then distributed on SDS-polyacrylamide gels (10%) and transferred to PVDF membranes (Millipore Corp., Billerica, MA) to perform the Western blotting test. 5% skim milk (in 150 mM NaCl, 0.1% Tween 20, 20 mM Tris-HCl pH 7.2) was utilized to block the PVDF membrane overnight at 4 °C, followed by the corresponding primary antibody incubation at 4 °C overnight. The membrane was washed three times with PBS at room temperature. The membranes were incubated via 1:10 000 diluted anti-mouse IgG secondary antibody (Abcam, Cambridge, MA) for 60 min. The protein expression level was detected with the enhanced chemiluminescence kit. The relative band intensities were compared to controls using Quantity One version 4.1.0.

RESULTS AND DISCUSSION

Molecular structure and characterization of complex 1. Targeted complex **1** was prepared via the reaction of $In(NO_3)_3{\cdot}6H_2O$ and 4,4′-dithiodibenzoic acid in the presence of NaOH as a pH modulator. It should be noted that the presence of NaOH has a major function in the formation of complex **1**, which is evidenced by the clear solution without the presence of NaOH along with the $[In_2NaO_6(H_2O)_6]$ clusters. The composition of **1** was completely determined via the energy spectrum analysis, scanning electron microscopy as well as EA. Based on the crystal data collected at room temperature, the structure of complex **1** was solved and refined. The results show that complex **1** is a part of a cubic crystal system with space group *Pn*-3*n*. According to the charge balance consideration as well as EA, the basic repeating unit of the molecule of **1** contains one sixth of the Na(I) ion, one third of the In(III) ion, a half of the $ddba^{2-}$ ligand, one coordinated water molecule, and one sixth of the NO_3^- ion. In the molecular unit, Na(I) along with In(III) ions have different coordination environments, although they are all six-coordinated (Fig. 1*a*). The In(III) ions placed in threefold symmetric crystallographic positions are surrounded by six oxygen donors in three different $ddba^{2-}$ ligands along with three water molecules, forming a distorted octahedral coordination environment. The Na(I) center coordination sphere is composed of carboxylate oxygen atoms of six different $ddba^{2-}$ ligands, which also shapes a distorted octahedral coordination environment. The In(III)–O bond distances are in the range 2.286(6) Å to 2.324(5) Å and the Na(I)–O bond length is 2.365(7) Å. A marked structural characteristic of complex **1** is the presence of a heterometallic trinuclear unit $[In_2NaO_6(H_2O)_6]$ acting as SBU. The quadruple symmetry $ddba^{2-}$ ligand was applied at the S–S bond center in crystallography. Each carboxylate was bridged by a μ_2–η^0:η^2 bridging mode. The two benzene rings make a dihedral angle of 89.9° (Fig. 1*b*). Thus, In(III) as well as Na (I) centers are linked via six μ_2–η^0:η^2 bridging carboxylic acid groups of six different $ddba^{2-}$ ligands, forming a linear $[In_2NaO_6(H_2O)_6]$ trinuclear unit in which the Na···In distance is 3.152(5) Å. The connection of $ddba^{2-}$ ligands with $[In_2NaO_6(H_2O)_6]$ trinuclear units forms a 3D framework with cavities that are large enough to accommodate the second cavity. Therefore, two identical networks penetrate each other, forming a two fold parallel penetrating frame. Compound **1** exhibits the solvent-contactable volume of 1621 $Å^3$ after two penetrations accounting for 15.2% of the crystal volume (Fig. 1*c*). From the topology point of view, the trinuclear $[In_2NaO_6(H_2O)_6]$ unit could be viewed as the 6-linked node, while the $ddba^{2-}$ ligand could be viewed as the two-coordinated node, Thus, the entire framework of **1** could be simplified into the six-linked **hxg** topological network and the Schläfli symbol is $(4^6.6^9)$ (Fig. 1*d*). The structure of **1** is similar to that of Cd(II)-based CP based on $[Cd_2NaO_6(H_2O)_6]$ SBU and a different flexible organic ligand [16].

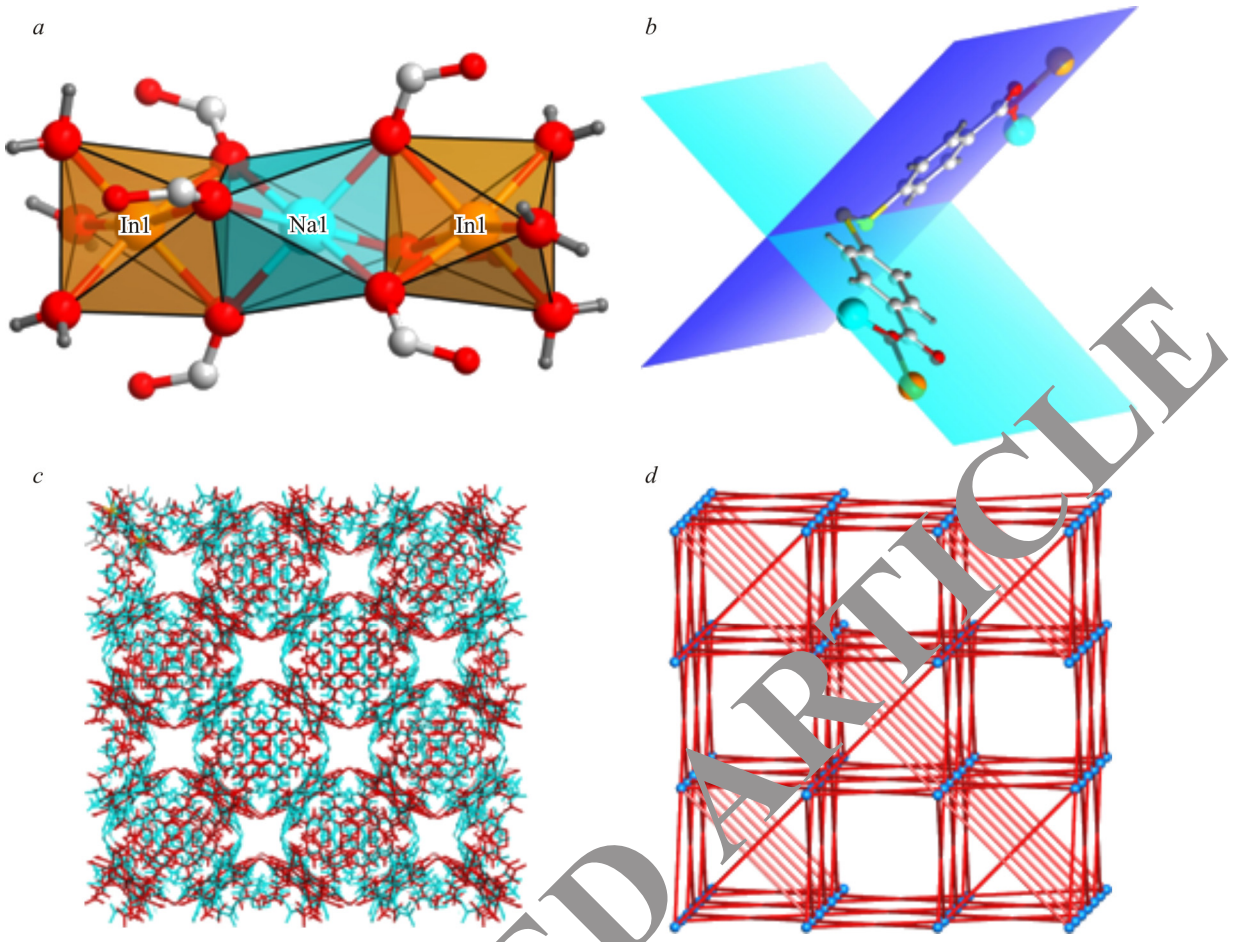

Fig. 1. View of the $[In_2NaO_6(H_2O)_6]$ cluster in **1** (*a*); view of the $ddba^{2-}$ ligand coordination pattern (*b*); view of the double interpenetrating network of **1** (*c*); view of the six-connected **hxg** topological network for **1** (*d*).

Powder XRD measurements, TGA profiles and nanosizing. For the sake of ascertaining the crystalline phase purity of complex **1**, powder XRD experiments were performed on complex **1**. It can be seen (Fig. 2*a*) that the powder XRD patterns of the bulk samples of **1** are in accordance with the simulated patterns from the single crystal data, demonstrating that a primary one crystalline phase exists in corresponding CP. In order to determine thermal stabilities of these complexes, TGA measurements were performed. TGA curve **1** shows that 16.4% of the first weight loss occurs in a range from 65 °C to 140 °C, due to the exclusion of several lattices as well as six coordination water components (calculated value: 16.1%). The remaining network of **1** can be thermally stabilized to about 300 °C (Fig. 2*b*). To confirm the presence of the Na(I) ion in the framework of **1**, the EDS analysis was performed using a JSM-6490 scanning electron microscope (Fig. 2*c*). The detected surface atomic ratio for Na and In is 1.98% and 4.97%, and the corresponding interior atomic ratio is 1.67% and 4.35%, which indicates that the Na and In atomic ratio is near to 1:2. Considering the following MTT assay experiments, it is essential to decrease crystal sizes of complex **1** to the nanometer level to facilitate the drug release into the body at the intravenous administration to be absorbed by specific tissues. The method of preparing nano-**1** was described in the experimental section. SEM and powder XRD measurements are remarkably crucial techniques which are employed to get important data about the shape, size, particle, and/or surface morphology of the prepared metal-organic compound and frameworks. Therefore, the skeleton integrity of the prepared samples was confirmed by powder XRD measurements, and the particle morphology was analyzed by JEOL-JEM-2010 F SEM. The SEM characterization reveals that nano-**1** are uniformly distributed nanorods with a mean thickness around 6075 nm (Fig. 2*d*).

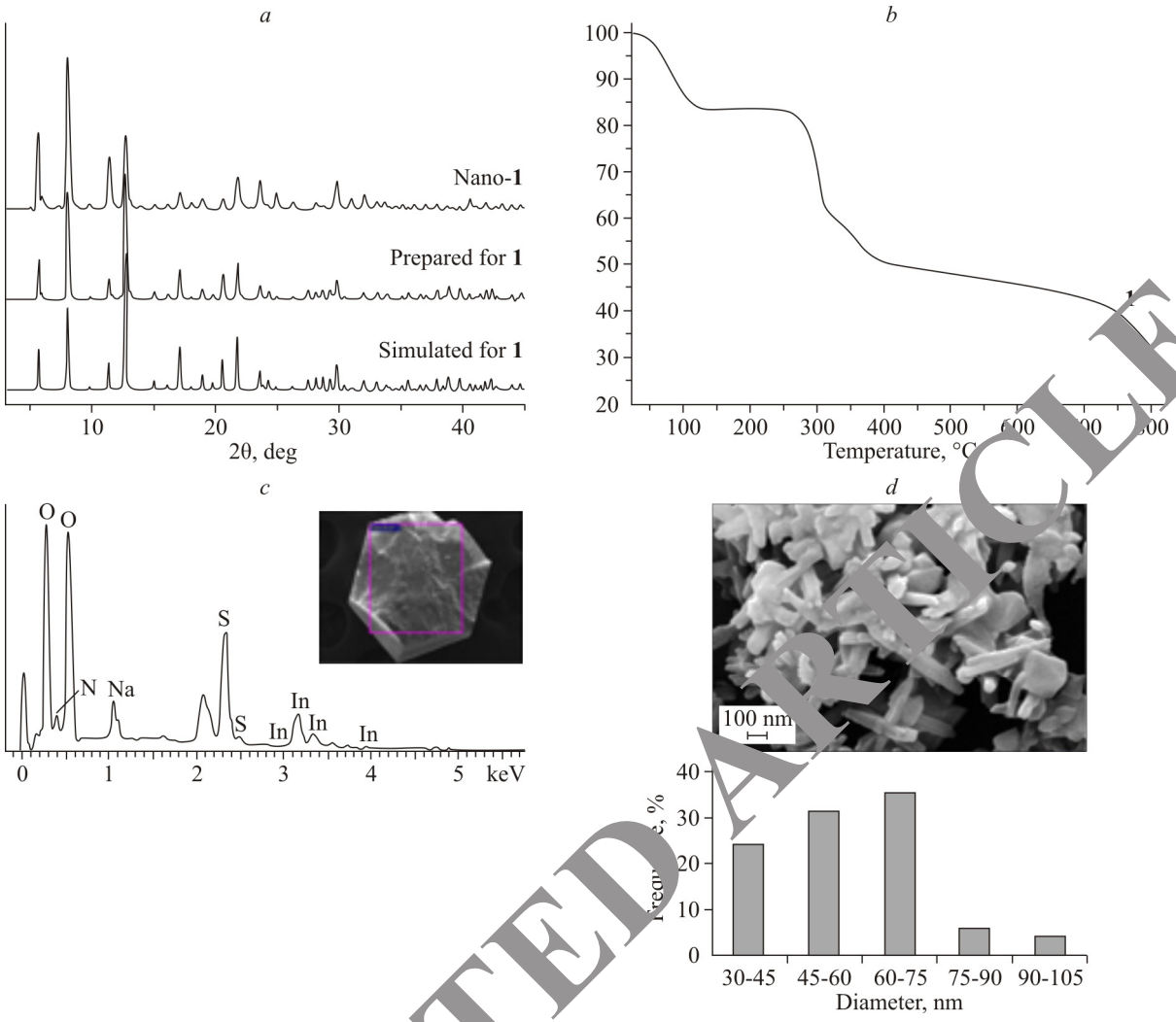

Fig. 2. Powder XRD patterns for complex **1** and nano-**1** (*a*); TGA curve of complex **1** (*b*); EDX analysis of **1** (*c*); SEM image of nano-**1** (*d*).

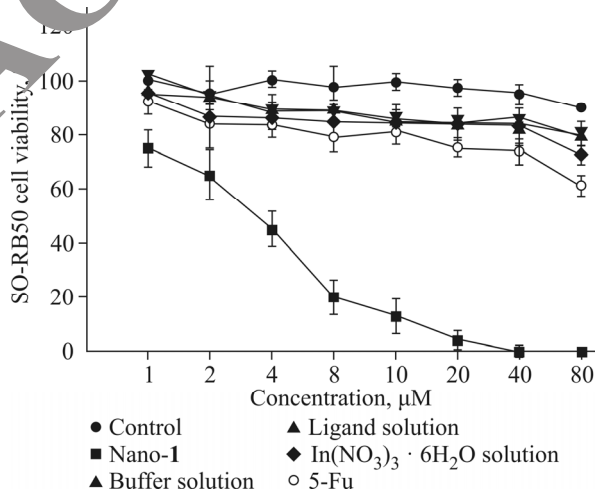

Fig. 3. Reduced retinoblastoma cell viability after treatment with nano-**1**. The 5-Fu resistance of SO-RB50 cells was treated by serious dilutions of nano-**1** for one day, and the cell viability was measured by the CCK-8 method.

TABLE 2. IC_{50} Values of the Compound Against SO-RB50 Cells. This Experiment Was Performed at Least Three Times

	Nano-**1**	Buffer solution	Ligand solution	$In(NO_3)_3 \cdot 6H_2O$ solution	5-Fu
IC_{50} (μM)	3.13±0.11	>80	>80	>80	>80

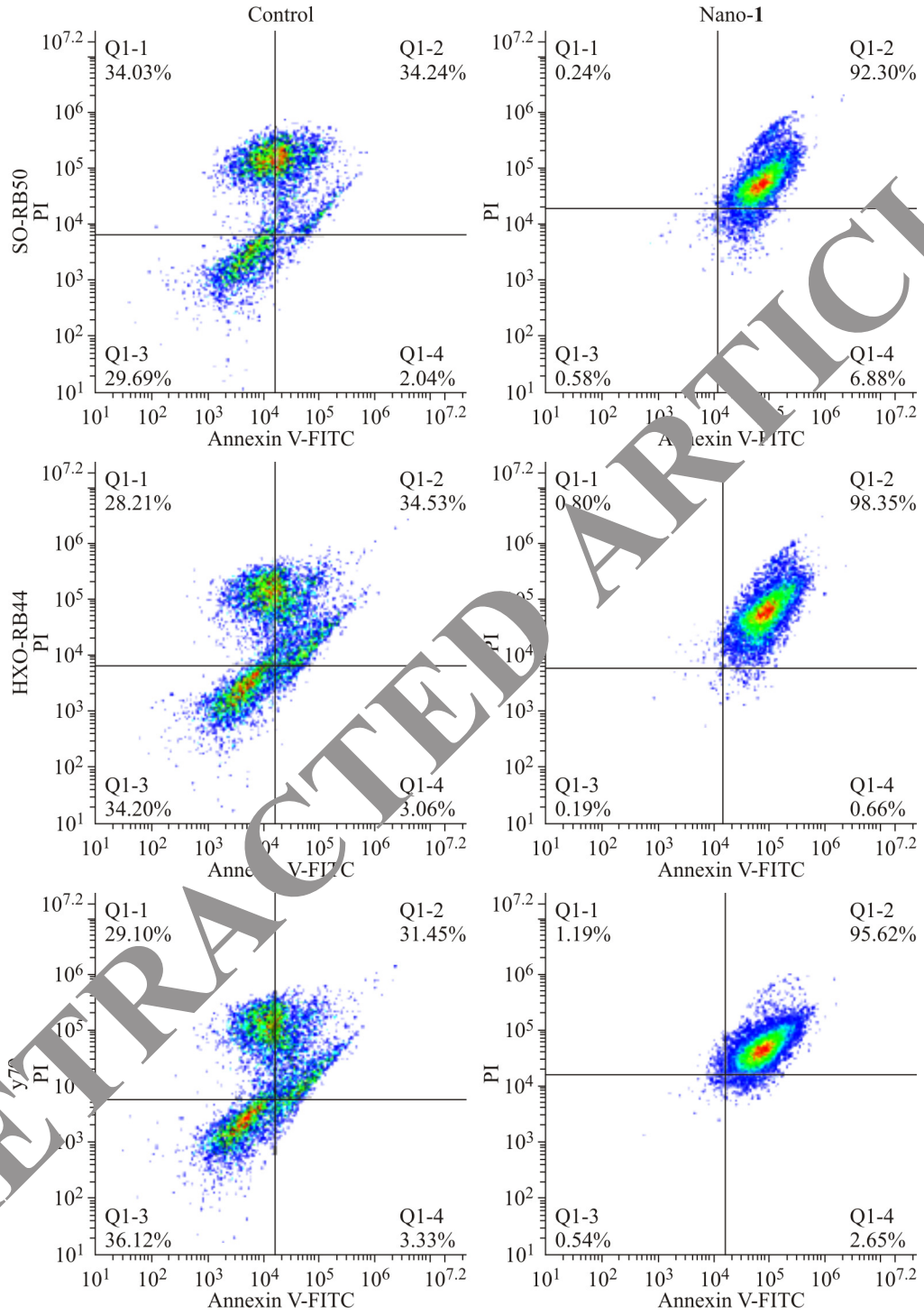

Fig. 4. Increased apoptotic percentage of SO-RB50, HXO-RB44, and y79 retinoblastoma cells after treatment with nano-**1**. The three cells were treated with nano-**1**, and the Annexin V-FITC/PI double staining assay was performed to detect the percentage of the cancer cells.

Cancer cell viability. After the design and synthesis of nano-**1** with a novel structure, the anticancer activity was further explored via the CCK-8 method. The SO-RB50 retinoblastoma cells were treated by a serious dilution of nano-**1** for one day. From Fig. 3 we can see that nano-**1** could only significantly reduce the cancer cell viability rather than the control solution. The nano-**1** inhibitory activity was even better than that of the positive control drug. These results indicate that nano-**1** exhibits a good anticancer activity against retinoblastoma cells in vitro. The IC_{50} values of this compound against retinoblastoma cells were calculated and listed in Table 2. The results reveal that nano-**1** has the lowest IC_{50} values and the best anticancer activity.

Nano-1 induces the apoptotic cell death in SO-RB50, HXO-RB44, and y79 retinoblastoma cells. As reported, most anticancer drugs exert activity on cancer cells mediated by the induction of cell apoptosis. In this research, we guessed that nano-**1** could also induce the cancer cell apoptosis and inhibit the cancer cell viability. The percentage of SO-RB50, HXO-RB44, and y79 retinoblastoma cells was measured after treating with nano-**1** by the Annexin V-FITC/PI double staining assay via a flow cytometer. From the results illustrated in Fig. 4 we can see that after the incubation with nano-**1** the rate of apoptotic cells significantly increased (92.30%, 98.35%, and 95.62%), which indicated the excellent anticancer activity of nano-**1** in vitro.

miR-16-1 miRNA expression level. In recent years, mi-RNAs were reported to play a vital important role in the existence and development of cancer cells. Especially, in the development of retinoblastoma, miR-16-1 takes a vital important place. Thus, the miR-16-1 relative expression in three different cell lines (SO-RB50, HXO-RB44, and y79) was detected by RT-PCR. From Fig. 5 we can see that the miR-16-1 expression in cancer cell lines is significantly higher than that in normal cells, while nano-**1** could significantly reduce the abnormally high miR-16-1 expression in these three cancer cell lines in a dose-dependent manner.

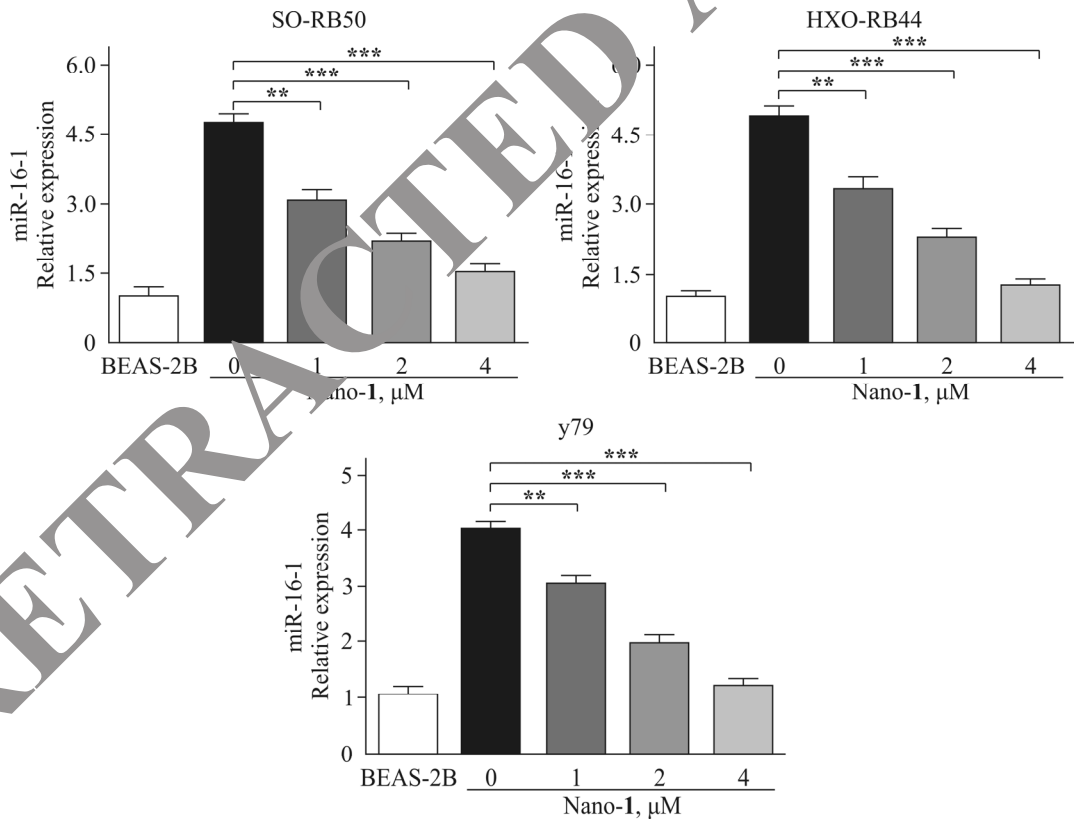

Fig. 5. Reduced miR-16-1 miRNA expression level after treatment with nano-**1**. SO-RB50, HXO-RB44, and y79 cancer cells were treated with nano-**1** with different concentrations. The relative miR-16-1 expression was measured by RT-PCR. All experiments were performed in triplicate. The data were shown as mean±SD.

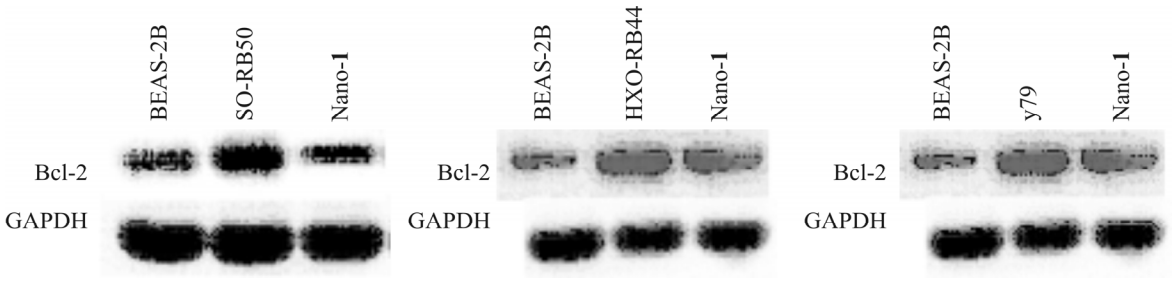

Fig. 6. Up-regulated Bcl-2 protein expression in cancer cells after treatment with nano-**1**. After treatment with nano-**1**, the Bcl-2 protein level in SO-RB50, HXO-RB44, and y79 was detected with the Western blot.

Bcl-2 expression level after treatment with nano-1. As reported, miR-16-1 could bind to 3′-UTR of Bcl-2 protein and regulate the physiological function of Bcl-2. Bcl-2 has a main function in cancer cell procession. Thus, to explore the mechanism of nano-**1** during cancer treatment, the Western blot was used to detect the Bcl-2 relative expression for SO-RB50, HXO-RB44, and y79 cells after treatment. From Fig. 6 we can see that the Bcl-2 relative expression level was lower in cancer cells compared with normal cells. However, nano-**1** obviously increased the Bcl-2 content in the retinoblastoma cell lines.

CONCLUSIONS

All in all, we have successfully prepared novel bimetallic CP using flexible 4,4′-dithiodibenzoic acid, which shows a 3D framework based on In_2Na cluster-based SBU. The chemical composition and the structure were characterized by EA, TGA, powder and single crystal X-ray diffraction. Furthermore, a process of sonochemistry with oleic acid treatment carried out at 453 K was used to produce nano-**1**. Furthermore, nano-**1** inhibits the miR-16-1 expression and then stimulates the Bcl-2 protein content in SO-RB50, HXO-RB44, and y79 retinoblastoma cells, and finally cause the apoptotic cell death. The Annexin V-FITC/PI staining results indicated that nano-**1** had excellent induction of the cancer cell apoptosis. In conclusion, nano-**1** has the potential of being a promising candidate for retinoblastoma treatment.

CONFLICT OF INTERESTS

The authors declare that they have no conflict of interests.

REFERENCES

1. F. Bray, J. Ferlay, I. Soerjomataram, R. L. Siegel, L. A. Torre, and A. Jemal. *Ca-Cancer J. Clin.*, **2018**, *68*, 394.
2. P. D. W. Eckford and F. C. Sharom. *Chem. Rev.*, **2009**, *109*, 2989.
3. P. M. Takahara, C. A. Frederick, and S. J. Lippard. *J. Am. Chem. Soc.*, **1996**, *118*, 12309.
4. S. Guo, R. Chen, M. Wei, H. Li, and Y. Liu. *IEEE Access*, **2018**, *6*, 45934.
5. W. Chen, L. Chang, S. B. Ren, Z. C. He, G. B. Huang, and X. H. Liu. *J. Hazard. Mater.*, **2020**, *384*, 121308.
6. J. Zhu and S. Luo. *Acta Mech.*, **2018**, *229*, 1703.
7. X. Feng, Y. Feng, N. Guo, Y. Sun, T. Zhang, L. F. Ma, and L. Y. Wang. *Inorg. Chem*., **2017**, *56,* 1713.
8. X. Feng, R. F. Li, L. Y. Wang, S. W. Ng, G. Z. Qin, and L. F. Ma. *CrystEngComm*, **2015**, *17,* 7878.
9. X. Feng, Y. Q. Feng, L. Liu, L. Y. Wang, H. L. Song, and S. W. Ng. *Dalton Trans*., **2013**, *42*, 7741.
10. S. Mukherjee, S. Ganguly, K. Manna, S. Mondal, S. Mahapatra, and D. Das. *Inorg. Chem.*, **2018**, *57*, 4050.
11. X. Du, R. Fan, L. Qiang, K. Xing, H. Ye, X. Ran, Y. Song, P. Wang, and Y. Yang. *ACS Appl. Mater. Interfaces*, **2017**, *9*, 28939.

12. B. Lei, M. Wang, Z. Jiang, W. Qi, R. Su, and Z. He. *ACS Appl. Mater. Interfaces*, **2018**, *10*, 16698.
13. G. M. Sheldrick. *Acta Crystallogr., Sect. C*, **2015**, *71*, 3.
14. H. Li, G. Gao, R. Chen, X. Ge, S. Guo, and L. Y. Hao. *Int. J. Software Eng. Know.*, **2019**, *29*, 93.
15. S. Guo, R. Chen, H. Li, T. Zhang, and Y. Liu. *Int. J. Software Eng. Know.*, **2019**, *29*, 139.
16. C. S. Liu, X. G. Yang, M. Hu, M. Du, and S. M. Fang. *Chem. Commun.*, **2012**, *48*, 7459.